PERGAMON

International Journal of Solids and Structures 38 (2001) 161–178

INTERNATIONAL JOURNAL OF SOLIDS and STRUCTURES

www.elsevier.com/locate/ijsolstr

Error analysis and adaptivity in three-dimensional linear elasticity by the usual and hypersingular boundary contour method

Yu Xie Mukherjee [a], Subrata Mukherjee [b,*]

[a] *DeHan Engineering Numerics, 39 Hickory Circle, Ithaca, NY 14850, USA*

[b] *Department of Theoretical and Applied Mechanics, 220 Kimball Hall, Cornell University, Ithaca, NY 14853-1503, USA*

Received 30 August 1999; in revised form 28 November 1999

Abstract

Two related topics are addressed in this article. The first part of the article proves that, for a certain admissible class of problems in linear elasticity, the hypersingular boundary contour method (HBCM) can be collocated at all boundary points on the surface of a three-dimensional (3-D) body, including those on boundary contours, edges and corners, because the HBCM-shape-functions satisfy, a priori, all the smoothness requirements for collocation at these points. In contrast, the hypersingular boundary element method needs, in general, relaxation of some of these smoothness requirements for its shape functions, even for collocation at regular points that lie on the boundaries of boundary elements.

A hypersingular residual, obtained from the standard and hypersingular boundary integral equations (HBIEs), has been recently proposed as a local error estimator for a boundary element, for the boundary integral equation. The second part in the present article is concerned with a definition of an analogous local error estimator for the boundary contour method, for 3-D linear elasticity. This error estimator is then used to drive an *h*-adaptive meshing procedure. Numerical results are presented to demonstrate adaptive meshing for selected example problems.

Keywords: Three-dimensional; Linear elasticity; Boundary contour method

1. Introduction

1.1. The boundary contour method

The usual boundary element method (BEM), for three-dimensional (3-D) linear elasticity, requires numerical evaluation of surface integrals on boundary elements on the surface of a body (see, e.g. Mukherjee, 1982). Nagarajan et al. (1994, 1996) have recently proposed a novel approach called the boundary

* Corresponding author. Tel.: +1-607-255-7143; fax: +1-607-255-2011.
E-mail address: sm85@cornell.edu (S. Mukherjee).

0020-7683/00/$ - see front matter
PII: S0020-7683(00)00005-6

contour method (BCM), that achieves a further reduction in dimension. The BCM, for 3-D linear elasticity problems, only requires numerical evaluation of line integrals over the closed bounding contours of the usual (surface) boundary elements.

The central idea of the BCM is the exploitation of the divergence-free property of the usual BEM integrand and a very useful application of Stokes' theorem, to analytically convert surface integrals on boundary elements to line integrals on closed contours that bound these elements. Lutz (1991) first proposed an application of this idea for the Laplace equation. Nagarajan et al. (1994) generalized this idea to linear elasticity. Numerical results for two-dimensional (2-D) problems, with linear boundary elements, are presented in Nagarajan et al. (1994), while results with quadratic boundary elements appear in Phan et al. (1997). 3-D elasticity problems, with quadratic boundary elements, is the subject of Nagarajan et al. (1996) and Mukherjee et al. (1997). Hypersingular boundary contour formulations, for 2-D (Phan et al., 1998) and 3-D (Mukherjee and Mukherjee, 1998) linear elasticity, have been proposed recently.

1.2. The hypersingular boundary element method

Hypersingular boundary element equations (HBIEs) are derived from a differentiated version of the usual boundary integral equations (BIEs). HBIEs have diverse important applications and are the subject of considerable current research (see, e.g. Krishnasamy et al., 1992; Tanaka et al., 1994; Paulino, 1995; Chen and Hong, 1999 for recent surveys of the field). HBIEs, e.g. have been employed for the evaluation of boundary stresses (e.g. Guiggiani et al., 1992; Wilde and Aliabadi, 1998; Zhao and Lan, 1999; Chati and Mukherjee, 1999), in wave scattering (e.g. Krishnasamy et al., 1990), in fracture mechanics (e.g. Gray et al., 1990; Lutz et al., 1992; Paulino, 1995; Gray and Paulino, 1998), to obtain symmetric Galerkin boundary element formulations (e.g. Bonnet, 1995; Gray et al., 1995; Gray and Paulino, 1997a,b), to obtain the hypersingular boundary contour method (Phan et al., 1998; Mukherjee and Mukherjee, 1998), to obtain the hypersingular boundary node method (Chati et al., 2000), and for error analysis (Paulino et al., 1996; Menon, 1996; Menon et al., 1999; Chati et al., 2000) and adaptivity (Chati et al., 2000). A lively debate (e.g. Martin and Rizzo, 1996; Cruse and Richardson, 1996), on smoothness requirements on boundary variables for collocating an HBIE on the boundary of a body, has apparently been concluded recently (Martin et al., 1998).

1.3. Local error estimates from the BIE and the HBIE

Paulino (1995) and Paulino et al. (1996) first proposed the idea of obtaining a hypersingular residual by substituting the BEM solution of a problem into the hypersingular BEM (HBEM) for the same problem; and then using this residual as an element error estimator in the BEM. It has been proved that (Menon, 1996; Menon et al., 1999), under certain conditions, this residual is related to a measure of the local error on a boundary element, and has been used to postulate local error estimates on that element. This idea has been applied to the collocation BEM (Paulino et al., 1996; Menon et al., 1999) and to the symmetric Galerkin BEM (Paulino and Gray, 1999). Very recently, residuals have been obtained in the context of the boundary node method (BNM) (Chati et al., 2000) and used to obtain local error estimates (at the element level) and then to drive an *h*-adaptive mesh refinement process. An analogous approach for error estimation and *h*-adaptivity, in the context of the BCM, is described in the present article.

1.4. Outline of the present paper

This article is organized as follows: The usual BCM and HBCM, for 3-D linear elasticity, is briefly reviewed first. The interesting question of collocating the hypersingular BIE, at edges and on corners on the boundary of a body, is discussed next. It is shown that, for problems within an admissible class defined later

in this article, the HBCM can be easily collocated at such irregular points (where the boundary of a body is not locally smooth) because the HBCM shape functions satisfy, a priori, all the smoothness requirements for collocation at an irregular point.

The next few sections of this article present the hypersingular residual as a measure of local error in the context of the BCM and HBCM, and an *h*-adaptive strategy driven by these error estimators. Numerical results for some selected examples follow. This article ends with some concluding remarks.

2. Boundary surface and boundary contour integral equations

A regularized form of the standard BIE (Rizzo, 1967), for 3-D linear elasticity, can be written as

$$0 = \int_{\partial B} \left[U_{ik}(\mathbf{x},\mathbf{y})\sigma_{ij}(\mathbf{y}) - \Sigma_{ijk}(\mathbf{x},\mathbf{y})\{u_i(\mathbf{y}) - u_i(\mathbf{x})\} \right] \mathbf{e}_j \cdot \mathrm{d}\mathbf{S}(\mathbf{y}) \equiv \int_{\partial B} \mathbf{F}_k \cdot \mathrm{d}\mathbf{S}(\mathbf{y}). \tag{1}$$

Here, ∂B is the bounding surface of a body B (B is an open set) with infinitesimal surface area $\mathrm{d}\mathbf{S} = \mathrm{d}S\mathbf{n}$, where $\mathbf{n}$ is the unit outward normal to ∂B at a point on it. The stress tensor is $\boldsymbol{\sigma}$, the displacement vector is $\mathbf{u}$ and $\mathbf{e}_j$ ($j = 1, 2, 3$) are global Cartesian unit vectors. The BEM Kelvin kernels are written in terms of (boundary) source points P and field points Q. These are

$$\Sigma_{ijk} = -\frac{1}{8\pi(1-\nu)r^2}\left[(1-2\nu)(r_{,i}\delta_{jk} + r_{,j}\delta_{ik} - r_{,k}\delta_{ij}) + 3r_{,i}r_{,j}r_{,k}\right], \tag{2}$$

$$U_{ik} = \frac{1}{16\pi\mu(1-\nu)r}\left[(3-4\nu)\delta_{ik} + r_{,i}r_{,k}\right] \tag{3}$$

in terms of r, the Eucleidian distance between the source and field points $\mathbf{x}$ and $\mathbf{y}$, and the shear modulus μ and Poisson's ratio ν of the isotropic elastic solid. Also, $\boldsymbol{\delta}$ is the Kronecker delta and $_{,i} = \partial/\partial y_i$. The range of indices in these and all other equations in this article is 1,2,3, unless specified otherwise.

It has been shown in Nagarajan et al. (1994, 1996) and Mukherjee et al. (1997) that the integrand vector $\mathbf{F}_k$ in Eq. (1) is divergence free (except at the point of singularity $P = Q$) and that the surface integral in it, over an open surface patch $S \in \partial B$, can be converted to a contour integral around the bounding curve C of S, by applying Stokes' theorem. Therefore, vectors $\mathbf{V}_k$ exist such that

$$\int_S \mathbf{F}_k \cdot \mathrm{d}\mathbf{S} = \oint_C \mathbf{V}_k \cdot \mathrm{d}\mathbf{r}. \tag{4}$$

Since the vectors $\mathbf{F}_k$ contain the unknown fields $\mathbf{u}$ and $\boldsymbol{\sigma}$, shape functions must be chosen for these variables, and potential functions derived for each linearly independent shape function, in order to determine the vectors $\mathbf{V}_k$. Also, as the kernels in Eq. (1) are functions only of $z_k = y_k - x_k$ (and not of the source and field coordinates separately), these shape functions must also be written in the coordinates z_k in order to determine the potential vectors $\mathbf{V}_k$. Finally, these shape functions are global in nature and are chosen to satisfy, a priori, the Navier–Cauchy equations of equilibrium. The weights, in linear combinations of these shape functions, however, are defined piecewise on boundary elements.

Quadratic shape functions are used in this work. With

$$z_k = y_k - x_k, \tag{5}$$

one has, on a boundary element

$$u_i = \sum_{\alpha=1}^{27} \beta_\alpha \overline{u}_{\alpha i}(y_1, y_2, y_3) = \sum_{\alpha=1}^{27} \hat{\beta}_\alpha(x_1, x_2, x_3)\,\overline{u}_{\alpha i}(z_1, z_2, z_3), \tag{6}$$

$$\sigma_{ij} = \sum_{\alpha=1}^{27} \beta_\alpha \overline{\sigma}_{\alpha ij}(y_1, y_2, y_3) = \sum_{\alpha=1}^{27} \hat{\beta}_\alpha (x_1, x_2, x_3)\, \overline{\sigma}_{\alpha ij}(z_1, z_2, z_3), \tag{7}$$

where $\overline{u}_{\alpha i}, \overline{\sigma}_{\alpha ij}$ (with $i = 1, 2, 3$ and $\alpha = 1, 2, \ldots, 27$) are the shape functions and β_α are the weights in the linear combinations of the shape functions. Each boundary element has, associated with it, 27 constants β_α, which will be related to physical variables on that element. This set of β's differ from one element to the next.

The displacement shape functions for $\alpha = 1, 2, 3$ are constants, those for $\alpha = 4, \ldots, 12$ are of first degree and those for $\alpha = 13, \ldots, 27$ are of second degree. There are a total of 27 linearly independent (vector) shape functions $\overline{\mathbf{u}}_\alpha$. The shape functions for the stresses are obtained from those for the displacements through the use of Hooke's law. The shape functions $\overline{u}_{\alpha i}$ and $\overline{\sigma}_{\alpha ij}$ are given in Mukherjee et al. (1997).

It is easy to show that the coordinate transformation (5) results in the constants $\hat{\beta}_j$ being related to the β_α's as follows:

$$\hat{\beta}_i = \sum_{\alpha=1}^{27} S_{i\alpha}(x_1, x_2, x_3)\, \beta_\alpha, \qquad i = 1, 2, 3, \tag{8}$$

$$\hat{\beta}_k = \sum_{\alpha=1}^{27} R_{n\alpha}(x_1, x_2, x_3)\, \beta_\alpha, \quad k = 4, 5, \ldots, 12, \;\; n = k - 3, \tag{9}$$

$$\hat{\beta}_\alpha = \beta_\alpha, \quad \alpha = 13, 14, \ldots, 27, \tag{10}$$

where

$$S_{i\alpha} = \overline{u}_{\alpha i}(x_1, x_2, x_3), \qquad i = 1, 2, 3, \;\; \alpha = 1, 2, \ldots, 27,$$

$$R_{k\alpha} = \left.\frac{\partial \overline{u}_{\alpha \ell}(y_1, y_2, y_3)}{\partial y_j}\right|_{(x_1, x_2, x_3)}, \qquad k = 1, 2, \ldots, 9, \;\; \alpha = 1, 2, \ldots, 27$$

with $j = 1 + \lfloor (k-1)/3 \rfloor$ and $\ell = k - 3j + 3$. Here, the symbol $\lfloor n \rfloor$, called the floor of n, denotes the largest integer less than or equal to n.

It is useful to note that the matrices $\mathbf{S}$ and $\mathbf{R}$ are functions of only the source point coordinates (x_1, x_2, x_3).

The procedure for designing boundary elements in the 3-D BCM is discussed in detail in Nagarajan et al. (1996) and Mukherjee et al. (1997). A set of primary physical variables a_k, whose number must match the number (here 27) of artificial variables β_k on a boundary element, are chosen first. The first step in the BCM solution procedure is to determine the unspecified primary physical variables in terms of those prescribed from the boundary conditions. Later, secondary physical variables as well as stresses, at boundary points, are obtained from a simple post-processing procedure. Unlike in the standard BEM, it is particularly easy to obtain surface variables, such as stresses and curvatures, in the BCM. This issue is discussed in Section 3.

A square invertible transformation matrix $\mathbf{T}$ relates the vectors $\mathbf{a}$ and $\boldsymbol{\beta}$ on element m according to the equation:

$$\overset{m}{a} = \overset{m}{T}\overset{m}{\beta}. \tag{11}$$

The CIM9 boundary element, shown in Fig. 1, is used in the present work. The displacement $\mathbf{u}$ is the primary physical variable at the three corner nodes C_i and the three midside nodes M_i, while tractions are primary variables at the internal nodes I_i. Thus, there are a total of 27 primary variables. The BCM equations are collocated at the six peripheral nodes as well as at the centroid of the element. In a typical discretization procedure, some of the peripheral nodes may lie on corners or edges, while the internal nodes are always located at regular points where the boundary ∂B is locally smooth. It is of an obvious advantage

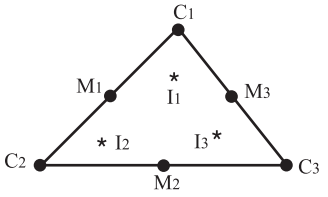

Fig. 1. The CIM9 boundary element.

to have to deal only with displacement components, that are always continuous, on edges and corners, while having traction components only at regular boundary points. It is important to restate that the BCM is versatile enough to handle any well-posed problem in linear elasticity – all the secondary variables can be easily determined by simple post-processing once the primary BCM equations are solved.

Details of the shape functions and intrinsic coordinates, that are used to define the geometry of the boundary elements, are available in Mukherjee et al. (1997). Also, the procedure for obtaining the vector potentials $\mathbf{V_k}$, for nonsingular as well as singular integrands, are available in Nagarajan et al. (1996) and Mukherjee et al. (1997). Finally, the regularized BIE, Eq. (1), is converted into a regularized BCE that can be collocated (as in the usual BEM) at any point (including those on edges and corners). This equation is

$$\begin{aligned} 0 = {} & \frac{1}{2}\sum_{m=1}^{M}\sum_{\alpha=13}^{27}\left[\oint_{L_m}\left(\overline{\sigma}_{\alpha ij}U_{ik}-\overline{u}_{\alpha i}\Sigma_{ijk}\right)\epsilon_{jnt}z_n\mathrm{d}z_t\right]\left[\overset{m}{T}{}^{-1}\overset{m}{a}\right]_{\alpha} \\ & +\sum_{m=1}^{M}\sum_{\alpha=4}^{12}\left[\oint_{L_m}\left(\overline{\sigma}_{\alpha ij}U_{ik}-\overline{u}_{\alpha i}\Sigma_{ijk}\right)\epsilon_{jnt}z_n\mathrm{d}z_t\right]\left[R\overset{m}{T}{}^{-1}\overset{m}{a}\right]_{\alpha-3} \\ & +\sum_{\substack{m=1\\ m\notin\mathscr{S}}}^{M}\sum_{\alpha=1}^{3}\left[\oint_{L_m}D_{\alpha jk}\mathrm{d}z_j\right]\left[S\left(\overset{m}{T}{}^{-1}\overset{m}{a}-\overset{P}{T}{}^{-1}\overset{P}{a}\right)\right]_{\alpha} \end{aligned} \tag{12}$$

with

$$\begin{aligned} \oint_{L_m}D_{\alpha jk}\mathrm{d}z_j = {} & -\int_{S_m}\Sigma_{\alpha jk}\mathbf{e}_j\cdot\mathrm{d}\mathbf{S} \\ = {} & \frac{1}{8\pi(1-\nu)}\oint_{L_m}\epsilon_{kij}\frac{r_{,\alpha}r_{,i}}{r}\,\mathrm{d}z_j+\frac{1-2\nu}{8\pi(1-\nu)}\oint_{L_m}\epsilon_{\alpha kj}\frac{1}{r}\mathrm{d}z_j+\frac{\Theta}{4\pi}\,\delta_{\alpha k}. \end{aligned} \tag{13}$$

Here, L_m is the bounding contour of the surface element S_m. In the above, Θ is the solid angle (subtended by a surface element m at a collocation point $\mathbf{x}$), which is defined as:

$$\Theta=\int_{S_m}\frac{\mathbf{r}\cdot\mathrm{d}\mathbf{S}}{r^3}. \tag{14}$$

Also, $\overset{m}{T}$ and $\overset{m}{a}$ are the transformation matrix and primary physical variable vectors on element m, $\overset{P}{T}$ and $\overset{P}{a}$ are the same quantities evaluated on any element that belongs to the set $\mathscr{S}$ of elements that contain the source point $\mathbf{x}$, and ϵ_{ijk} is the usual alternating symbol.

The procedure for obtaining an assembled discretized form of Eq. (12) is described in Mukherjee et al. (1997) and Mukherjee and Mukherjee (1998). The final result is

$$Ka=0, \tag{15}$$

which is written as

$$Ax=By, \tag{16}$$

where **x** contains the unknown and **y** the known (from the boundary conditions) values of the primary physical variables on the surface of the body. Once these equations are solved, the vector **a** is completely known. Now, at a post processing step, $\overset{m}{\beta}_{\alpha}$ can be easily obtained on each boundary element from Eq. (11).

3. Hypersingular boundary surface and boundary contour integral equations

A HBIE can be obtained by differentiating the standard BIE *at an internal point*, with respect to the coordinates of this internal source point. A regularized version of this equation, containing, at most, weak singular integrals, is (see, e.g. Cruse and Richardson (1996) for a detailed discussion):

$$0 = \int_{\partial B} U_{ik,n}(\mathbf{x},\mathbf{y})\big[\sigma_{ij}(\mathbf{y}) - \sigma_{ij}(\mathbf{x})\big] n_j(\mathbf{y}) \mathrm{d}S(\mathbf{y}) - \int_{\partial B} \Sigma_{ijk,n}(\mathbf{x},\mathbf{y})[u_i(\mathbf{y}) - u_i(\mathbf{x}) - u_{i,\ell}(\mathbf{x})(y_\ell - x_\ell)] n_j(\mathbf{y}) \mathrm{d}S(\mathbf{y}). \tag{17}$$

Martin et al. (1998, Appendix II2, p. 905) have proved that Eq. (17) can be collocated even at an edge or corner point **x** on the surface of a 3-D body, provided that the displacement and stress fields in Eq. (17) satisfy certain smoothness requirements. This issue is discussed further in Section 4 of this article. Such points, at which the bounding surface of a body is not locally smooth, are henceforth referred to as irregular points. Conversely, the boundary of a body is locally smooth at a regular point. Further, a regular surface point can lie on a contour (regular contour point, RCP) or away from a contour (regular off-contour boundary point, ROCBP). A point inside a body is called an internal point.

The regularized HBIE (17) can be converted to a regularized hypersingular boundary contour equation (HBCE). Details are available in Mukherjee and Mukherjee (1998). The result is:

$$\begin{aligned}
0 = & -\sum_{m=1}^{M}\sum_{\alpha=13}^{27}\left[\oint_{L_m}\left(\overline{\sigma}_{\alpha ij}U_{ik} - \overline{u}_{\alpha i}\Sigma_{ijk}\right)\epsilon_{jnt}\mathrm{d}x_t\right]\left[\overset{m}{T}{}^{-1}\overset{m}{a}\right]_{\alpha} \\
& +\sum_{m=1}^{M}\sum_{\alpha=4}^{12}\left[\oint_{L_m}\left(\overline{\sigma}_{\alpha ij}U_{ik} - \overline{u}_{\alpha i}\Sigma_{ijk}\right)\epsilon_{jst}x_s\mathrm{d}x_t\right]\left[R_{,N}\overset{m}{T}{}^{-1}\overset{m}{a}\right]_{\alpha-3} \\
& -\sum_{\substack{m=1\\ m\notin\mathscr{S}}}^{M}\sum_{\alpha=4}^{12}\left[\oint_{L_m}\left(\overline{\sigma}_{\alpha ij}U_{ik} - \overline{u}_{\alpha i}\Sigma_{ijk}\right)\epsilon_{jnt}\mathrm{d}x_t\right]\left[R\left(\overset{m}{T}{}^{-1}\overset{m}{a} - \overset{P}{T}{}^{-1}\overset{P}{a}\right)\right]_{\alpha-3} \\
& +\sum_{\substack{m=1\\ m\notin\mathscr{S}}}^{M}\sum_{\alpha=1}^{3}\left[\oint_{L_m}D_{\alpha jk}\mathrm{d}x_j\right]\left[S_{,N}\left(\overset{m}{T}{}^{-1}\overset{m}{a} - \overset{P}{T}{}^{-1}\overset{P}{a}\right)\right]_{\alpha} \\
& +\sum_{\substack{m=1\\ m\notin\mathscr{S}}}^{M}\sum_{\alpha=1}^{3}\left[\oint_{L_m}\Sigma_{\alpha jk}\epsilon_{jnt}\mathrm{d}x_t\right]\left[S\left(\overset{m}{T}{}^{-1}\overset{m}{a} - \overset{P}{T}{}^{-1}\overset{P}{a}\right)\right]_{\alpha},
\end{aligned} \tag{18}$$

where, as before, $\mathscr{S}$ is the set of boundary elements that contains the source point **x**. The derivatives $R_{,N}$ and $S_{,N}$ in Eq. (18) are taken with respect to the source point coordinates x_n. In Eq. (18), the integrands in the first two terms are regular (O(1)). The third and fourth (potentially strongly singular, $O(1/r)$) as well as the fifth (potentially hypersingular, $O(1/r^2)$) need to be evaluated only on nonsingular elements.

4. Collocation of the HBCE at an irregular surface point

4.1. The HBIE (17)

Let ∂B_n, $(n = 1, 2, 3, \ldots, N)$ be smooth pieces of ∂B that meet at an irregular point $\mathbf{x} \in \partial B$. Also, let a source point, with coordinates x_k, be denoted by P, and a field point, with coordinates y_k, be denoted by Q.

Martin et al. (1998) state the following requirements for collocating the HBIE (17) at an irregular point $P \in \partial B$. These are

(i) The displacement $\mathbf{u}$ must satisfy the equilibrium equations in B.
(ii) (a) The stress $\boldsymbol{\sigma}$ must be continuous in B.
(b) The stress $\boldsymbol{\sigma}$ must be continuous on ∂B.
(iii) $|\mathbf{u}(Q_n) - \mathbf{u}^L(Q_n; P)| = \mathrm{O}(r_n^{(1+\alpha)})$ as $r_n \to 0$, for each n.
(iv) $[\sigma_{ij}(Q_n) - \sigma_{ij}(P)]n_j(Q_n) = \mathrm{O}(r_n^{\alpha})$ as $r_n \to 0$, for each n.

In the above, $r_n = |\mathbf{y}(Q_n) - \mathbf{x}(P)|, Q_n \in \partial B_n$, and $\alpha > 0$. Also,

$$u_i^L(Q_n; P) = u_i(P) + u_{i,j}(P)[y_j(Q_n) - x_j(P)]. \tag{19}$$

There are two important issues to consider here.

The first is that, if there is to be any hope for collocating (17) at an irregular point P, the exact solution of a boundary value problem must satisfy conditions (i)–(iv). Clearly, one should not attempt this collocation if, for example the stress is unbounded at P (this can easily happen – see an exhaustive study on the subject in Glushkov et al. (1999)), or is bounded but discontinuous at P (e.g. at the tip of a wedge – see, e.g. Zhang and Mukherjee (1991)). The discussion in the rest of this article is limited to the class of problems, *referred to as the admissible class*, whose exact solutions satisfy conditions (i)–(iv).

The second issue refers to smoothness requirements on the shape functions for $\mathbf{u}$, $\boldsymbol{\sigma}$ and the traction $\boldsymbol{\tau} = \mathbf{n} \cdot \boldsymbol{\sigma}$ in Eq. (17). The simpler case of collocating Eq. (17) at a RCP is considered first. It is very difficult, in practice, to find BEM shape functions that satisfy, a priori, conditions (ii(b))–(iv) (modified to suit a RCP – see Martin et al., 1998, p. 901) at a RCP on the surface of a 3-D body of arbitrary shape. Hence, the search for the so-called "relaxed smoothness requirements", i.e. allowing violation of some of the (modified) conditions (ii(b)–iv), for shape functions at isolated RCPs on ∂B. This topic has been the subject of intense debate (e.g. Cruse and Richardson, 1996; Martin and Rizzo, 1996). The current thinking (Martin et al., 1998) is that, while relaxed smoothness strategies violate strict mathematical requirements, such sins might, in fact, be forgivable in a clever (e.g. based on Eq. (51) in Martin et al., 1998) numerical implementation of the HBIE. Researchers (e.g. Huang and Cruse, 1994; Cruse and Richardson, 1996; Richardson et al., 1997; Liu and Chen, 1999), have been able to get satisfactory numerical results with such "relaxation strategies".

The situation, of course, is more complex if one desires to collocate Eq. (17) at an irregular point P on ∂B. Martin et al. (1998) feel that the requirements (i)–(iv) are more stringent in this case, although the authors of this article feel that this issue demands further research.

4.2. The HBCE (18)

The HBCE (18) is based on the shape functions given in Eqs. (6)–(7). The shape functions have both a global (they are initially defined as functions of $\mathbf{y}$) as well as a local (the weights β_k are only defined piecewise on the boundary elements) character.

Consider a singular boundary element containing the source and field points P and Q, with P, an irregular point on ∂B. Let this element be any one of the smooth pieces of ∂B that meet at P. From Eqs. (6)–(7), it is easy to show that

$$u_i(Q) - u_i^L(Q;P) = u_i(Q) - u_i(P) - u_{i,j}(P)[y_j(Q) - x_j(P)] = \sum_{\alpha=13}^{27} \beta_\alpha \bar{u}_{\alpha i}(\mathbf{z}) = \mathrm{O}(r^2), \tag{20}$$

$$\sigma_{ij}(Q) - \sigma_{ij}(P) = \sum_{\alpha=13}^{27} \beta_\alpha \bar{\sigma}_{\alpha ij}(\mathbf{z}) = \mathrm{O}(r), \tag{21}$$

where $r = |\mathbf{y}(Q) - \mathbf{x}(P)| = |\mathbf{z}|$. The last equalities in the above equations are true, in view of the fact, that the shape functions $\bar{u}_{\alpha i}$ and $\bar{\sigma}_{\alpha ij}$ are quadratic and linear, respectively, in z_k, for $\alpha = 13, 14, \ldots, 27$ (Mukherjee et al., 1997, Table 1). Note that these weights β_α belong to the element containing P and Q and are unique on that element (see below Eq. (7)).

As an aside, it is interesting to connect with Toh and Mukherjee (1994, p. 2304), where, for the same problem, the requirement $|\nabla\mathbf{u}(Q) - \nabla\mathbf{u}(P)| = \mathrm{O}(r^\alpha)$ is prescribed as $r \to 0$. It is easy to show that (Mukherjee and Mukherjee, 1998), for the BCM shape functions on a singular element:

$$u_{i,j}(Q) - u_{i,j}(P) = \sum_{\alpha=4}^{12} [R_{,J}(\mathbf{x})\beta]_{\alpha-3} \bar{u}_{\alpha i}(\mathbf{z}) = \mathrm{O}(r) \tag{22}$$

as $\bar{u}_{\alpha i}(\mathbf{z})$ is linear in $\mathbf{z}$ for $\alpha = 4, 5, \ldots, 12$.

In view of Eqs. (20)–(21), conditions (iii)–(iv) in Section 4.1 are satisfied a priori by the BCM shape functions defined by Eqs. (6)–(7). Satisfaction of condition (ii(b)) on ∂B follows from Eq. (21). The conditions inside B (i and ii(a)), of course, have nothing to do with BEM shape functions that are only defined on the bounding surface ∂B, but rather with the boundary element method itself. The BCM is derived from the BEM, and it satisfies these internal point conditions in the same way as does the BEM. (As a bonus, the BCM shape functions satisfy the Navier–Cauchy equilibrium equations of linear elasticity a priori (see, below, Eq. (4)), although weights are not defined at points $p \in B$.) Please note that the above arguments have been made for the "worst case scenario" of the collocation point $P \in \partial B$ being an *irregular* point. Of course, these arguments also go through for regular points (on or off contour) on ∂B.

In view of the above, all the conditions (i)–(iv) are satisfied a priori by the BCM, and there is no need to consider "relaxed smoothness requirements" in this method. It is worth repeating again that it is extremely difficult to find, in general, BEM shape functions (for 3-D elasticity problems) that satisfy conditions (ii(b))–(iv) a priori. The primary reason for this is that BEM shape functions are defined only on the bounding surface of a body, while the BCM ones are defined in B (although the weights are defined only on ∂B).

4.3. Numerical results

The HCBE (18) was first presented in Mukherjee and Mukherjee (1998) but numerical results from this equation were not presented in that article. This is done for the first time below.

First, please note that Eq. (18) has two free indicies, k and n, so that it represents nine equations. These equations arise from $u_{k,n}$ (please see the detailed derivation of Eqs. (17) and (18) in Mukherjee and Mukherjee (1998). Different strategies are possible for collocating Eq. (18) at a boundary point. The first is to use all nine equations. The second is to use six corresponding to $\epsilon_{kn} = (1/2)(u_{k,n} + u_{n,k})$. The six equation strategy amounts to replacing E_{kn}, the right-hand side of Eq. (18), by $(1/2)(E_{kn} + E_{nk})$. Both the nine and six equation strategies lead to overdetermined systems, but are convenient for collocating at irregular boundary points since the source point normal is not involved in these cases. A third, the three equation strategy, suitable for collocation at regular points, corresponds to the traction components τ_n. In this case, the right-hand side (E_{kn}) of Eq. (18) is replaced by $[\lambda E_{mm}\delta_{kn} + \mu(E_{kn} + E_{nk})]n_k(P)$, where λ and μ are Lamé constants, δ_{ij} are components of the Kronecker delta and Hooke's law is used. The three equation strategy involving the traction components is not convenient for collocating the HBCE at a point on an edge or a

corner of a body where the normal to the body surface has a jump discontinuity. In view of the assumed continuity of the stress tensor at such a point, this situation leads to a jump in traction at that point, unless the stress tensor is zero there. One would, therefore, need to use multiple source points, each belonging to a smooth surface meeting at that irregular point, and collocate separately at these points. Since the primary purpose here is to demonstrate collocation of Eq. (18) at irregular boundary points, only the nine and six equation strategies are used below.

It should be mentioned here that, for the HBCM in 2-D elasticity, a strategy corresponding to the first one above has been successfully employed by Phan et al. (1998) and a strategy corresponding the third one above has been implemented by Zhou et al. (1999).

The overdetermined system of linear algebraic equations, resulting from the nine and six equation strategies mentioned above, have been solved by using a subroutine based on QR decomposition of the system matrix. This subroutine has been obtained form the IMSL software package.

Numerical results have been obtained for a sample problem of a hollow sphere, under internal pressure. The inner and outer radii of the sphere are one and two units, respectively, the shear modulus $\mu = 1$ and Poisson's ration $v = 0.3$. The internal pressure is 1.

One-eighth of the sphere is modeled with a surface mesh shown in Fig. 2. The mesh used in this work has 36 elements on each flat surface and 36 elements on each curved surface, for a total of 180 surface elements. It is seen from Fig. 2 that many of the collocation points lie on edges and six of them lie on corners of the surface of the one-eighth sphere.

Numerical results, for the radial displacement in the sphere, are shown as functions of the radius (along the x_1 axis) in Fig. 3. In this figure, the BCM and HBCM results are compared with the exact solution of the problem (Timoshenko and Goodier, 1970). The first and last points along the axis lie on corners, the rest lie along an edge. The agreement between the exact, BCM and nine equation HBCM solution is seen to be excellent.

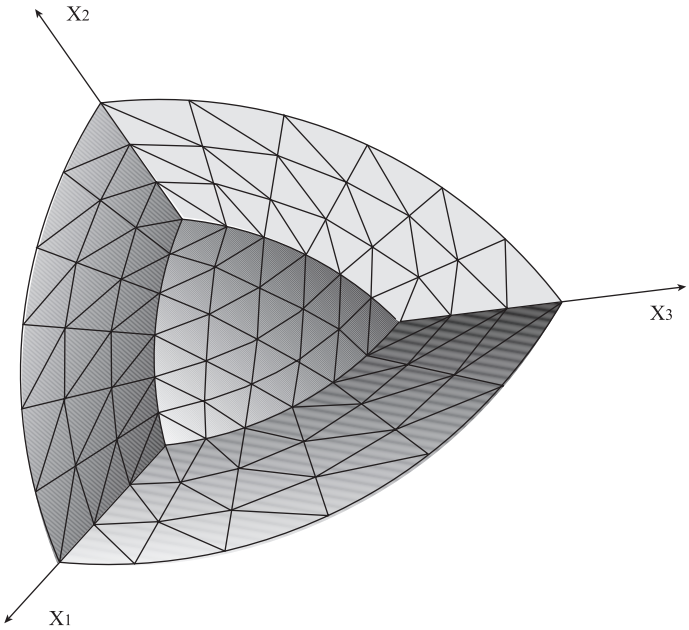

Fig. 2. A typical mesh on the surface of a one-eighth sphere.

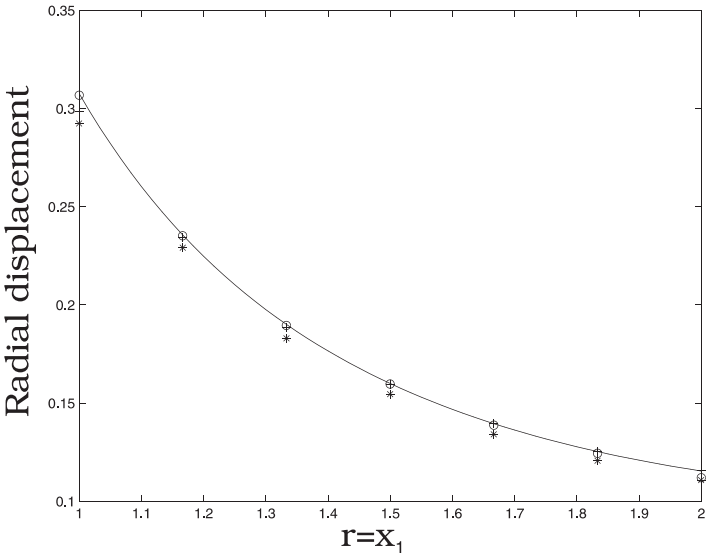

Fig. 3. Hollow sphere under internal pressure. Radial displacement as a function of radius along the x_1 axis. Exact solution: —, BCM solution: ∘, six equation HBCM solution: ∗, nine equation HBCM solution: +.

5. Error analysis and adaptive meshing

5.1. Hypersingular residuals as local error estimators

The idea of using hypersingular residuals, to obtain local error estimates for the BIE, was first proposed by Paulino (1995) and Paulino et al. (1996). This idea has been applied to the collocation BEM (Paulino et al., 1996; Menon et al., 1999), to the symmetric Galerkin BEM (Paulino and Gray, 1999) and to the BNM (Chati et al., 2000). The main idea, applied to the BCM, is as follows:

The usual BCM Eq. (12) is solved first for the boundary variables (tractions and displacements) **a**. Next, this value of **a** is input into the right hand side of Eq. (18) in order to obtain the hypersingular residuals v_{kn} in the displacement gradients $u_{k,n}$. Next, the stress residuals are obtained from Hooke's law:

$$s_{kn} = \lambda v_{mm}\delta_{kn} + \mu(v_{kn} + v_{nk}). \tag{23}$$

Finally, a scalar measure r of the residual, evaluated at the centroid of a triangular surface element, is postulated based on the idea of energy. This is

$$r = s_{kn}v_{kn}. \tag{24}$$

It has been proved by Menon et al. (1999) for the BIE that, under certain favorable conditions, real positive constants c_1 and c_2 exist such that

$$c_1 r \leqslant \epsilon \leqslant c_2 r, \tag{25}$$

where r is some scalar measure of a hypersingular residual and ϵ is a scalar measure of the exact local error. Thus, a hypersingular residual is expected to provide a good estimate of the local error on a boundary element. It should be mentioned here that the definitions of the residuals used in Menon et al. (1999) are analogous to, but different in detail from, the ones proposed in this article.

In the rest of this article, $e = r$, where r, defined in Eq. (24) (and evaluated at an element centroid), is the hypersingular residual, and e is the local element error estimator that is used to drive an h-adaptive procedure with the BCM.

5.2. Adaptive meshing strategy

The flow chart for adaptive meshing is shown in Fig. 4.

The remeshing strategy is based on the values of the error estimator e at each element centroid. This strategy is shown in Fig. 5 in which $\bar{e}$ is the average value of the error estimator e over all the boundary elements.

A possible criterion for stopping cell refinement can be

$$\bar{e} \leqslant e_{\text{global}}, \tag{26}$$

where e_{global} has a preset value that depends on the level of overall desired accuracy.

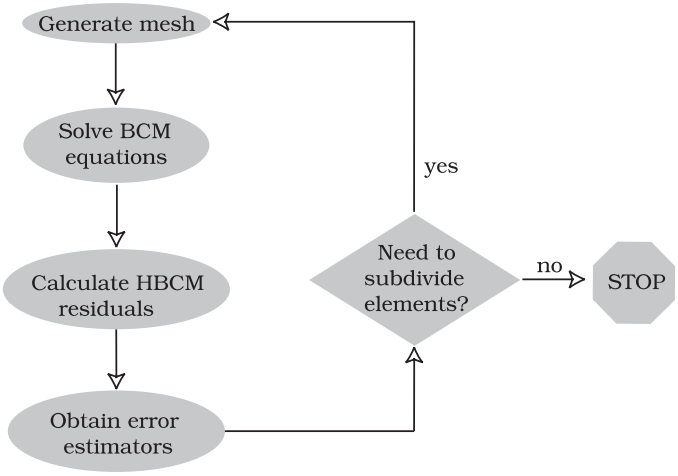

Fig. 4. Flow chart for adaptive meshing.

$\gamma = e/\bar{e}$	$1 \leqslant \gamma < 2$	$2 \leqslant \gamma < 3$	$3 \leqslant \gamma$
	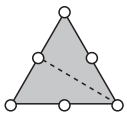	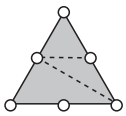	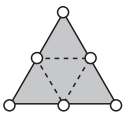
One element is split into	2 elements	3 elements	4 elements

Fig. 5. Remeshing strategy.

5.3. Numerical results

5.3.1. Example one – short clamped cylinder under tension

The first example is concerned with a short cylinder, which is clamped at the bottom and subjected to unit tensile traction on the top surface (Fig. 6(a)). The radius and length of the cylinder are each two units, the shear modulus of the cylinder material is 1.0 and the Poisson's ratio is 0.3 (in consistent units). The initial mesh on the top (loaded) and bottom (clamped) faces of the cylinder are identical and are shown in Fig. 6(b) as the initial uniform mesh on its curved surface is shown in Fig. 7(b).

It is known (Cruse, 1969; Pickett, 1944) that, for this problem, the normal stress component σ_{33} varies slowly over much of the clamped face, but exhibits sharp gradients near its boundary. This stress component becomes singular on the boundary of the clamped face. The behavior of the shearing stress com-

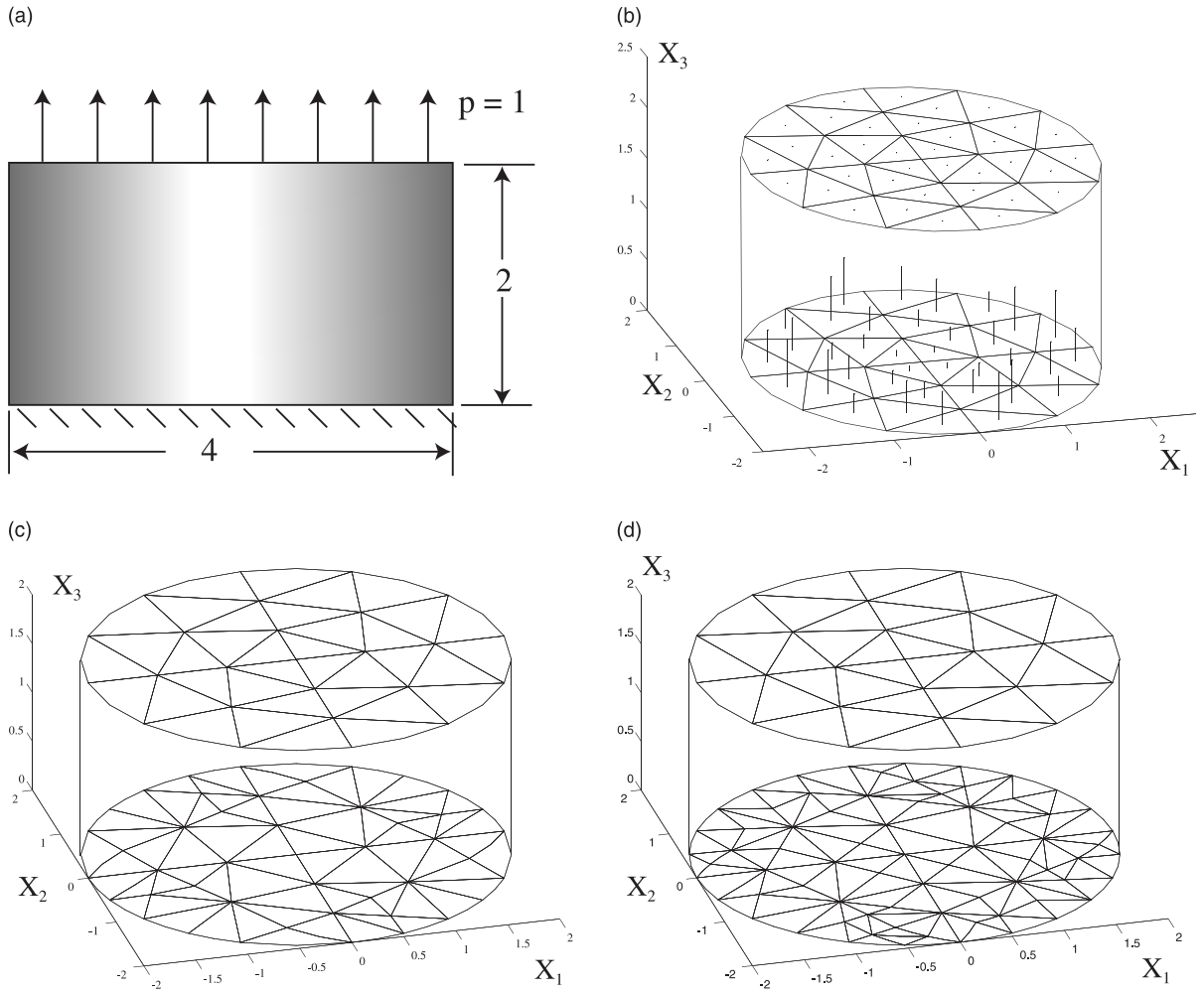

Fig. 6. Adaptive meshing of the top and bottom faces of a clamped cylinder under tension: (a) geometry and loading, (b) initial mesh with element error estimators, (c) mesh at the end of the first adaptive step and (d) mesh at the end of the second adaptive step.

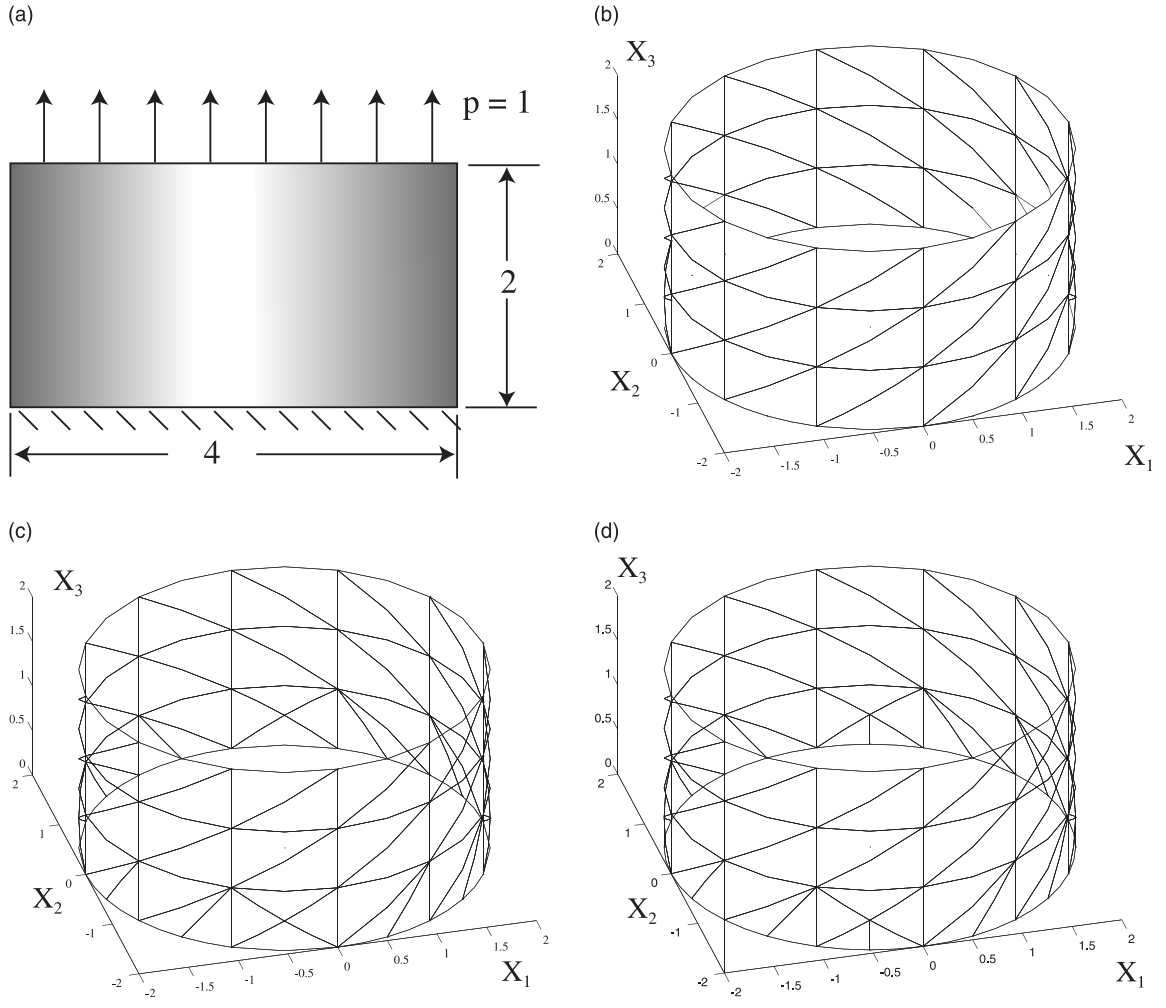

Fig. 7. Adaptive meshing of the curved surface of a clamped cylinder under tension: (a) geometry and loading, (b) initial uniform mesh, (c) mesh at the end of the first adaptive step and (d) mesh at the end of the second adaptive step.

ponent σ_{zr} (here $r, \theta, z \equiv 3$ are the usual polar coordinates) on the clamped face is qualitatively similar to that of σ_{33}. The stresses are uniform on the loaded face.

It is seen from Figs. 6 and 7 that this behavior is captured well by the adaptive scheme. Element error estimators are obtained from Eqs. (18), (23) and (24) after first averaging the traction results from Eq. (12) within each element and then using these averaged traction values. Fig. 6(b) shows that these element error estimators are largest on the elements near the boundary of the clamped face. As a consequence (Fig. 6(b)–(d)), the region near the boundary of the clamped face is refined most but the mesh on the loaded face of the cylinder is left unaltered. Also, Fig. 7(c) and (d) shows that some mesh refinement takes place on the bottom layer of the curved surface of the cylinder, which is nearest to the clamped face, while the rest of the mesh on it remains unaltered.

Finally, the mesh statistics, together with $\bar{e}$, the average value of the error estimator e over the entire surface of the cylinder, appear in Table 1. As expected, $\bar{e}$ is seen to decrease with mesh refinement.

Table 1
Mesh statistics and $\bar{e}$ for the clamped cylinder under tension

Mesh	No. of elements	No. of nodes	$\bar{e}$
Initial	144	290	0.0086799
After first adaptive step	192	386	0.0048994
After second adaptive step	246	494	0.0042723

5.3.2. Example two – Lamé problem for a hollow cylinder

This example is concerned with a thick hollow cylinder, in plane strain, subjected to external radial tensile loading. The inner and outer radii of the hollow cylinder are one and three units, respectively. The shear modulus of the material is 1.0, the Poisson's ratio is 0.3 and the external radial traction is 3 (in consistent units). A quarter of the cylinder is modeled and the initial mesh on the quarter cylinder is shown in Fig. 8. The bars in Fig. 8 are the error estimators evaluated at the centroids of the boundary elements. As expected (Paulino et al., 1997; also, please see the discussion in the following paragraph), the error estimators are largest on the surface of the hole and on the elements on the upper and lower surfaces (EBAF and HCDG) of the cylinder that lie near the hole. (The visible elements are shown in Fig. 8 and the hidden ones are not.)

The next (and final) mesh, obtained from the adaptive strategy outlined in Sections 5.1 and 5.2 above, is shown in Fig. 9. Mesh refinement is carried out vigorously on the upper and lower surfaces EBAF and HCDG of the cylinder (the hidden elements are not shown in Fig. 9), as well as on the surface FADG of the hole, while the symmetry planes ABCD and EFGH, on which the stresses are independent of the x_3 coordinate, are only slightly refined in order to maintain mesh compatibility. Of course, refinement of the surfaces EBAF and HCDG is expected in view of the presence of radial stress gradients on these surfaces. The situation on the curved surface FADG is particularly interesting. In this axisymmetric problem, the tangential gradients of the stress fields in the θ direction are, of course, always zero. It is important to note, however, that the radial stress gradients are large at points on the hole surface, and this fact leads to large error estimators and significant refinement of the boundary elements on the surface FADG. The corresponding 2-D case is discussed, in some detail, in Paulino et al. (1997).

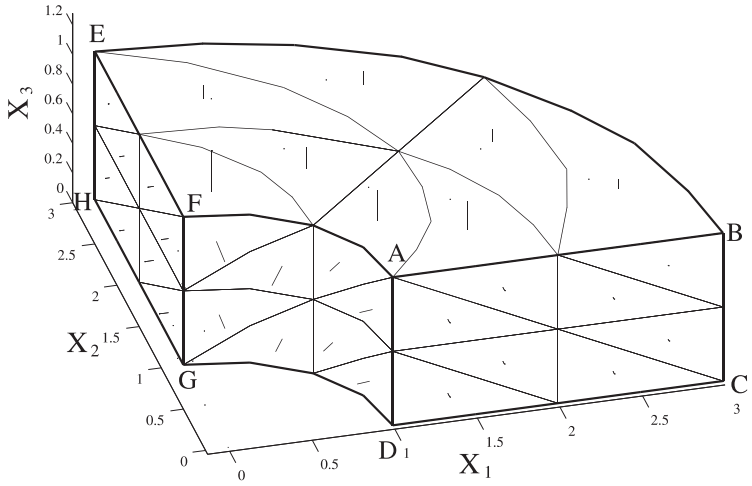

Fig. 8. Lamé problem – initial mesh on the quarter cylinder together with element error estimators.

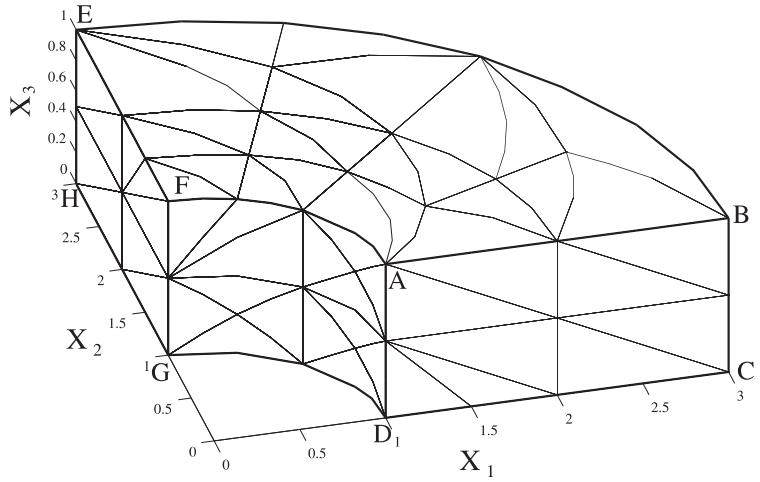

Fig. 9. Lamé problem – final mesh on the quarter cylinder.

It is important to check the behavior of the actual errors, when the exact solution is available, in adaptive meshing problems such as this example. The tangential stress $\sigma_{\theta\theta}$, as a function of the radial distance r from the center of the cylinder, is shown in Fig. 10. The solid line in Fig. 10 is the exact solution (from, e.g. Timoshenko and Goodier, 1970) while the numerical results, from the initial and the final mesh, are designated by open circles and plus signs, respectively. The numerical results for the tangential stress are obtained from the calculated tractions at the traction nodes I_i (see Fig. 1) on the boundary elements on the symmetry face ABCD in Figs. 8 and 9. The inaccurate results from the initial crude mesh is a consequence of the chosen mesh, not the method itself. This can be seen, for example, by observing the BCM results for

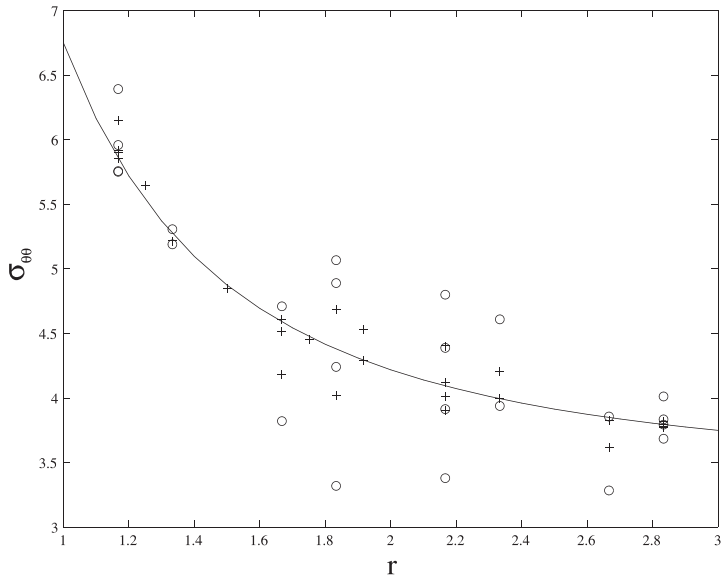

Fig. 10. Lamé problem for a hollow cylinder. Tangential stress $\sigma_{\theta\theta}$ as a function of radial distance r. Exact solution: —, BCM solution from initial mesh: ∘, BCM solution from final mesh: +.

the Lamé problem for a hollow sphere under internal pressure in Fig. 3 (open circles), obtained from a reasonably fine mesh; as well as by examining other numerical results from the BCM, in, e.g. Mukherjee et al. (1997).

The $\mathscr{L}_2$ error in a numerical solution in Fig. 10 is defined as

$$\epsilon = \frac{100}{\bar{\sigma}_{\theta\theta}} \sqrt{\frac{\sum_{i=1}^{n} (\epsilon_i)^2}{n}}, \tag{27}$$

where the pointwise error $\epsilon_i = (\sigma_{\theta\theta})^{(i)}_{\text{numerical}} - (\sigma_{\theta\theta})^{(i)}_{\text{exact}}$ at node i, n is the number of nodes and $\bar{\sigma}_{\theta\theta}$ is the average value of the exact solution for $\sigma_{\theta\theta}$ (here 4.5). The resulting values of the $\mathscr{L}_2$ errors are 9.83% and 3.83% for the initial and final mesh, respectively. The adaptive meshing procedure is seen to reduce the error significantly in one step.

6. Concluding remarks

This article has presented two topics related to the boundary contour method: The first is a proof of the fact that the shape functions of the hypersingular boundary contour method, used in this work, satisfy, a priori, all the smoothness requirements for collocation at any point on the boundary of a body, provided that the exact solution of the problem satisfies conditions (i)–(iv) in Section 4.1. The second is the use of an error estimator, previously employed in the context of the boundary element method, for the estimation of element-based errors in the BCM; and then carrying out adaptive meshing driven by these estimators. Two numerical examples illustrate the efficacy of the proposed method. The reader is also referred to Chati et al. (2000) for a discussion of adaptivity in the context of the boundary node method.

Acknowledgements

This research was supported by the NSF SBIR Phase II grant DMI-9629076 to DeHan Engineering Numerics.

References

Bonnet, M., 1995. Regularized direct and indirect symmetric variational BIE formulations for three-dimensional elasticity. Engng. Anal. Bound. Elem. 15, 93–102.

Chati, M.K., Mukherjee, S., 1999. Evaluation of gradients on the boundary using fully regularized hypersingular boundary integral equations. Acta Mech. 135, 41–45.

Chati, M.K., Paulino, G.H., Mukherjee, S., 2000. The meshless standard and hypersingular boundary node methods – applications to error estimation and adaptivity in three-dimensional problems, submitted for publication.

Chen, J.T., Hong, H-K., 1999. Review of dual boundary element methods with emphasis on hypersingular integrals and divergent series. ASME Appl. Mech. Rev. 52, 17–33.

Cruse, T.A., 1969. Numerical solutions in three-dimensional elastostatics. Int. J. Solids Struct. 5, 1259–1274.

Cruse, T.A., Richardson, J.D., 1996. Non-singular Somigliana stress identities in elasticity. Int. J. Numer. Meth. Engng. 39, 3273–3304.

Glushkov, E., Glushkova, N., Lapina, O., 1999. 3-D elastic stress analysis at polyhedral corner points. Int. J. Solids Struct. 36, 1105–1128.

Gray, L.J., Martha, L.F., Ingraffea, A.R., 1990. Hypersingular integrals in boundary element fracture analysis. Int. J. Numer. Meth. Engng. 29, 1135–1158.

Gray, L.J., Balakrishna, C., Kane, J.H., 1995. Symmetric Galerkin fracture analysis. Engng. Anal. Bound. Elem. 15, 103–109.

Gray, L.J., Paulino, G.H., 1997a. Symmetric Galerkin boundary integral formulation for interface and multizone problems. Int. J. Numer. Meth. Engng. 40, 3085–3101.

Gray, L.J., Paulino, G.H., 1997b. Symmetric Galerkin boundary integral fracture analysis for plane orthotropic elasticity. Comput. Mech. 20, 26–33.

Gray, L.J., Paulino, G.H., 1998. Crack tip interpolation revisited. SIAM J. Appl. Math. 58, 428–455.

Guiggiani, M., Krishnasamy, G., Rudolphi, T.J., Rizzo, F.J., 1992. A general algorithm for the numerical solution of hypersingular boundary integral equations. ASME J. Appl. Mech. 59, 604–614.

Huang, Q., Cruse, T.A., 1994. On the nonsingular traction BIE in elasticity. Int. J. Numer. Meth. Engng. 37, 2041–2072.

Krishnasamy, G., Schmerr, L.W., Rudolphi, T.J., Rizzo, F.J., 1990. Hypersingular boundary integral equations: some applications in acoustic and elastic wave scattering. ASME J. Appl. Mech. 57, 404–414.

Krishnasamy, G., Rizzo, F.J., Rudolphi, T.J., 1992. Hypersingular boundary integral equations: their occurrence, interpretation, regularization and computation. In: Banerjee, P.K., Kobayashi, S. (Eds.), Developments in Boundary Element Methods-7. Elsevier Applied Science, London, pp. 207–252.

Liu, Y., Chen, S., 1999. A new form of the hypersingular boundary integral equation for 3-D acoustics and its implementation with C^0 elements. Comput Methods Appl. Mech. Engng. 173, 375–386.

Lutz, E.D., 1991. Numerical Methods for Hypersingular and Near-Singular Boundary Integrals in Fracture Mechanics. Ph.D. dissertation, Cornell University, Ithaca, NY.

Lutz, E.D., Ingraffea, A.R., Gray, L.J., 1992. Use of 'simple solutions' for boundary integral methods in elasticity and fracture analysis. Int. J. Numer. Meth. Engng. 35, 1737–1751.

Martin, P.A., Rizzo, F.J., 1996. Hypersingular integrals: how smooth must the density be? Int. J. Numer. Meth. Engng. 39, a687–704.

Martin, P.A., Rizzo, F.J., Cruse, T.A., 1998. Smoothness-relaxation strategies for singular and hypersingular integral equations. Int. J. Numer. Meth. Engng. 42, 885–906.

Menon, G., 1996. Hypersingular error estimates in boundary element methods. M.S. Thesis, Cornell University, Ithaca, NY.

Menon, G., Paulino, G.H., Mukherjee, S., 1999. Analysis of hypersingular residual error estimates in boundary element methods for potential problems. Comput Methods Appl. Mech. Engng. 173, 449–473.

Mukherjee, S., 1982. Boundary Element Methods in Creep and Fracture, Elsevier, London.

Mukherjee, Y.X., Mukherjee, S., Shi, X., Nagarajan, A., 1997. The boundary contour method for three-dimensional linear elasticity with a new quadratic boundary element. Engng. Anal. Bound. Elem. 20, 35–44.

Mukherjee, S., Mukherjee, Y.X., 1998. The hypersingular boundary contour method for three-dimensional linear elasticity. ASME J. Appl. Mech. 65, 300–309.

Nagarajan, A., Lutz, E.D., Mukherjee, S., 1994. A novel boundary element method for linear elasticity with no numerical integration for 2-D and line integrals for 3-D problems. ASME J. Appl. Mech. 61, 264–269.

Nagarajan, A., Mukherjee, S., Lutz, E.D., 1996. The boundary contour method for three-dimensional linear elasticity. ASME J. Appl. Mech. 63, 278–286.

Paulino, G.H., 1995. Novel Formulations of the Boundary Element Method for Fracture Mechanics and Error Estimation. Ph.D. dissertation, Cornell University, Ithaca, NY.

Paulino, G.H., Gray, L.J., Zarkian, V., 1996. Hypersingular residuals – a new approach for error estimation in the boundary element method. Int. J. Numer. Meth. Engng. 39, 2005–2029.

Paulino, G.H., Shi, F., Mukherjee, S., Ramesh, P., 1997. Nodal sensitivities as error estimates in computational mechanics. Acta Mech. 121, 191–213.

Paulino, G.H., Gray, L.J., 1999. Galerkin residuals for adaptive symmetric-Galerkin boundary element methods. ASCE J. Engng. Mech. 125, 575–585.

Phan, A-V., Mukherjee, S., Mayer, J.R.R., 1997. The boundary contour method for two-dimensional linear elasticity with quadratic boundary elements. Comput. Mech. 20, 310–319.

Phan, A-V., Mukherjee, S., Mayer, J.R.R., 1998. The hypersingular boundary contour method for two-dimensional linear elasticity. Acta Mech. 130, 209–225.

Pickett, G., 1944. Application of the Fourier method to the solution of certain boundary value problems in the theory of elasticity. Trans. ASME J. Appl. Mech. 66, A176–A182.

Richardson, J.D., Cruse, T.A., Huang, Q., 1997. On the validity of conforming BEM algorithms for hypersingular boundary integral equations. Comput. Mech. 20, 213–220.

Rizzo, F.J., 1967. An integral equation approach to boundary value problems of classical elastostatics. Qly. Appl. Math. 25, 83–95.

Tanaka, M., Sladek, V., Sladek, J., 1994. Regularization techniques applied to boundary element methods. ASME Appl. Mech. Rev. 47, 457–499.

Timoshenko, S.P., Goodier, J.N., 1970. Theory of Elasticity, 3rd. ed. McGraw Hill, New York.

Toh, K-C., Mukherjee, S., 1994. Hypersingular and finite part integrals in the boundary element method. Int. J. Solids Struct. 31, 2299–2312.

Wilde, A.J., Aliabadi, M.H., 1998. Direct evaluation of boundary stresses in the 3D BEM of elastostatics. Commun. Numer. Methods Engng. 14, 505–517.

Zhang, Q., Mukherjee, S., 1991. Design sensitivity coefficients for linear elastic bodies with zones and corners by the derivative boundary element method. Int. J. Solids Struct. 27, 983–998.

Zhao, Z.Y., Lan, S.R., 1999. Boundary stress calculation – a comparison study. Comput. Struct. 71, 77–85.

Zhou, S., Cao, Z., Sun, S., 1999. The traction boundary contour method for linear elasticity. Int. J. Numer. Meth. Engng. 46, 1883–1895.